Composite Structures 160 (2017) 185–194

Contents lists available at ScienceDirect

Composite Structures

journal homepage: www.elsevier.com/locate/compstruct

A strain gage technique for the determination of mixed mode stress intensity factors of orthotropic materials

Debaleena Chakraborty, D. Chakraborty *, K.S.R.K. Murthy

Mechanical Engineering Department, Indian Institute of Technology Guwahati, 781039, India

ARTICLE INFO

Article history:
Received 27 July 2016
Revised 28 September 2016
Accepted 16 October 2016
Available online 18 October 2016

Keywords:
Orthotropic
Mixed mode
Stress intensity factor
Strain gage
Radial location

ABSTRACT

A theoretical frame work is developed for strain gage based determination of mixed mode (K_I/K_{II}) stress intensity factors (SIFs) in slant edge cracked plate (SECP) made of orthotropic materials. Using three parameter strain series around the crack tip and appropriate stress functions, the present formulation shows that mixed mode SIFs in orthotropic materials could be determined using only four strain gages. A finite element based methodology is developed to determine the upper bound on the radial location (r_{max}) of strain gages ensuring accurate determination of SIFs. Proposed technique is applied to numerical simulation of $[0_2/90]_{2S}$ and $[0/\pm45/90]_S$ glass-epoxy SECP laminates to demonstrate accurate determination of mixed mode SIFs by placing the gages within r_{max}. Results from the present work provide clear guidelines in terms of number of strain gages and their suggested locations for accurate determination of mixed mode SIFs in orthotropic materials.

1. Introduction

Fracture mechanics based analysis of orthotropic materials has been an important area of research in general and the pioneering work towards the development of fracture mechanics studies of orthotropic materials was started by Irwin [1] in 1962. Various other researchers have taken these works further ahead [2–7]. Due to the limitation of analytical methods in dealing with general crack propagations and inconsistent geometrical and boundary conditions, several numerical and experimental techniques were developed by various researchers for solving fracture mechanics problems of orthotropic materials under mode I and mixed mode loading. Various numerical methods such as modified crack closure technique (MCCT) and displacement correlation technique (DCT) by Kim and Paulino [8], extended finite element method (XFEM) by Asadpoure and Mohammadi [9] and strong formulation finite element method (SFEM) based on generalized differential quadrature (GDQ) by Fantuzzi et al. [10] etc. to name a few have been employed for accurate prediction of SIFs of orthotropic laminates. In experimental analysis of anisotropic materials various techniques have been reported for measurement of fracture parameters. Baik et al. [11] used the method of caustics to obtain SIFs in orthotropic materials under mode I and mixed mode static loading conditions. Yao et al. [12] studied the stress singularities of mode I crack tip in orthotropic composites using the reflective caustic technology. Mojtahed and Zachary [13] devised a method for obtaining mode I SIF in orthotropic materials by using photoelastic technique. Ju and Liu [14] have used the technique of coherent grading sensing (CGS) interferometry to experimentally determine SIF for cracked composite panels (unidirectional graphite-epoxy) under bending (plane-stress deformation). Khanna et al. [15] used the technique of transmission photoelasticity to determine the SIF for cracks in composites. Mogadpalli and Parameswaran [16] investigated on the application of digital image correlation (DIC) to determine SIF for cracks in orthotropic composites.

The use of strain gages also forms an important segment in assessment of fracture parameters because of their economic and handling feasibility. However, various factors such as high strain gradients, finite gage size, 3D effects posed limitations in accurate determination of SIFs using strain gages. The single strain gage based determination of mode I SIF (K_I) of isotropic materials proposed by Dally and Sanford [17] in 1987 (DS technique) took care of most of the aforementioned difficulties by employing three parameter strain series equations. Consequently, various other researchers reported strain gage based methods for the determination of SIFs for either isotropic or orthotropic materials [18–25]. Amongst them, Shukla et al. [21] were the first to propose a technique for the determination of K_I of orthotropic materials employing two parameter strain field expressions around the crack tip. Khanna and Shukla [22] formulated the use of strain gages in

* Corresponding author.
E-mail addresses: debaleena@iitg.ernet.in (D. Chakraborty), chakra@iit.ernet.in (D. Chakraborty), ksrkm@iitg.ernet.in (K.S.R.K. Murthy).

http://dx.doi.org/10.1016/j.compstruct.2016.10.044
0263-8223/

accurate estimation of dynamic SIFs provided the gages are pasted within the singularity dominated zone (SDZ). Chakraborty et al. [24,25] were the first to propose an extension of the DS technique to orthotropic laminates with single-ended and double-ended cracks.

Frequent occurrence of mixed mode conditions can be attributed to the orientations which a crack generally makes with the loading direction. Researchers have numerically verified the partition of fracture modes on rigid interfaces in orthotropic laminated double cantilever beams (DCB) under general loading conditions that include crack tip bending moments, axial and shear forces [26,27]. In spite of frequent occurrence of mixed mode conditions, very few works have been reported with regard to strain gage based determination of mixed mode SIFs (K_I, K_{II}) even in case of isotropic materials. For example, Dally and Berger (DB technique) [28,29] were the first to propose an approach involving a strain series with more number of parameters than that proposed in the DS technique thus enabling the strain gages to be located at distances further away from the crack tip. Dorogoy and Rittel [30] employed a three strain gage rosette to measure K_I and K_{II} by considering a three parameter strain series. Sarangi et al. [31] proposed modified DB technique incorporating more number of parameters in the strain series for determination of K_I and K_{II} of isotropic materials.

Strain gage based applications require strain gages to be placed at locations away from the crack tip and the measured strains are then equated with suitable analytical expressions to extract the SIFs. However, the extent of radial distance of the strain gage from the crack tip is important as it dictates whether the selected analytical expression can be represented by the measured strains. Moreover, 3D effects and high strain gradients affect the accuracy of the measured strains if the strain gage(s) are placed very near to the crack tip [17,21,32]. In case of orthotropic materials, the radial distance of the strain gages should be at least equal to the thickness of the plate to avoid the 3D effects [21]. Sarangi et al. [26] estimated the permissible extent of the radial locations of strain gages ensuring accurate determination of mixed mode SIFs in isotropic materials. Chakraborty et al. [24,25] reported estimation of valid radial locations and orientation for a strain gage ensuring accurate estimation of K_I in orthotropic laminates. Small gage length gages are used to minimize the strain gradients effect [17,29].

Therefore, while development of suitable methodology for strain gage based determination of SIFs is important, it is also extremely important that the locations and orientations of the strain gages are known apriori ensuring accurate determination of SIF. Literature review reveals that though there are number of papers on determination of SIFs using strain gages and minimizing the number of strain gages for isotropic materials, there are only a counted few for orthotropic materials. In addition, analysis of notched/cracked composites has been an important area of research from the view point of delamination initiation from such notches/cracks under loading. Even though there has been numerical work on prediction of delamination initiation from such notches/cracks [33–35], in spite of the fact that strain gage based determination of SIFs is simple [36], there have been few works available in this direction [21–23]. One of the reasons for this is the fact that unlike isotropic materials, there has been lack of proper theoretical development for orthotropic materials supporting strain gage based determination of SIFs and providing guidelines for exact number of strain gages required and their locations facilitating accurate measurement of SIFs. Only recently, based on Irwin's stress function Chakraborty et al. [24] extended the DS technique [17] and proposed an appropriate theoretical development for measurement of K_I using a single strain gage. But till date, there has been no theoretical development reported for providing guidelines in measurement of mixed mode SIFs (K_I/K_{II}) for orthotropic materials using minimum number of strain gages and their recommended location, whereas the same has been developed for isotropic materials [29,31]. Therefore, the present paper aims at developing a suitable analytical framework for determination of mixed mode (I/II) SIFs using minimum number of strain gages in an orthotropic laminate. It also aims to propose a methodology to determine the maximum radial location (r_{max}) within which the strain gages should be placed to ensure accurate determination of K_I and K_{II} using a three parameter strain series. Numerical simulations performed to substantiate the theoretical development are also presented which will provide guidelines and recommendations in terms of number of strain gages to be used and their optimal radial locations ensuring accurate values of K_I and K_{II} for conducting strain gage based experiments for a given configuration. The paper is organized as follows; the theoretical formulations are presented in Section 2. Section 3 gives detailed analysis of the numerical simulations and the corresponding results. Section 4 presents the concluding remarks.

2. Theoretical formulation

2.1. Strain gage techniques for determination of K_I and K_{II}

In 2D bodies, mixed mode loading indicates simultaneous occurrence of opening mode (mode I) and shearing mode (mode II) for which both K_I and K_{II} are required to describe the conditions near the crack tip. Employing the Westergaard's approach, Irwin [1,2] suggested stress functions for symmetric and skew-symmetric loading for orthotropic materials. For orthotropic materials, the present work uses the modified mode I stress function proposed by Shukla and co-workers [21] in line with the generalized Westergaard approach [37] as

$$F_I = \frac{1}{2}\left\{\mathrm{Re}\overline{\overline{Z}}_I(z_1) + \mathrm{Re}\overline{\overline{Z}}_I(z_2)\right\} - \frac{\beta}{2\alpha}\left\{\mathrm{Re}\overline{\overline{Z}}_I(z_1) - \mathrm{Re}\overline{\overline{Z}}_I(z_2)\right\} - \frac{\beta}{2\alpha}\left\{\mathrm{Re}\overline{\overline{Y}}_I(z_1) - \mathrm{Re}\overline{\overline{Y}}_I(z_2)\right\} \quad (1)$$

For mode II, the modified stress function as per generalized Westergaard approach [37] may be written as

$$F_I = \frac{1}{2}\left\{\mathrm{Re}\overline{\overline{Y}}_{II}(z_1) + \mathrm{Re}\overline{\overline{Y}}_{II}(z_2)\right\} - \frac{1}{2\alpha}\left\{\mathrm{Im}\overline{\overline{Z}}_{II}(z_1) - \mathrm{Im}\overline{\overline{Z}}_{II}(z_2)\right\} - \frac{1}{2\alpha}\left\{\mathrm{Re}\overline{\overline{Y}}_{II}(z_1) - \mathrm{Re}\overline{\overline{Y}}_{II}(z_2)\right\} \quad (2)$$

where $\overline{Z}_{I,II}(z_i)$ and $\overline{\overline{Z}}_{I,II}(z_i)$ are the first and second integrals with respect to $z_i (i = 1, 2)$ of a complex function $Z(z_i)$ and $z_i (i = 1, 2)$ is given by

$$z_1 = x + iy_1 = x + i(\beta + \alpha)y = r_1 e^{i\theta_1} \text{ and } z_2 = x + iy_2 = x + i(\beta - \alpha)y = r_2 e^{i\theta_2} \quad (3)$$

and, $Y_{I,II}(z_i)$ is another analytical function used in conjunction with the standard Westergaard stress function $Z(z_i)$. Additionally, other parameters are defined as

$$\tan\theta_1 = (\beta + \alpha)\tan\theta; \quad \tan\theta_2 = (\beta - \alpha)\tan\theta$$
$$r_1^2 = r^2(\cos^2\theta + (\beta + \alpha)^2 \sin^2\theta); \quad r_2^2 = r^2(\cos^2\theta + (\beta - \alpha)^2 \sin^2\theta)$$
$$2\beta^2 = \frac{a_{66} + 2a_{12}}{2a_{11}} + \sqrt{\frac{a_{22}}{a_{11}}}; \quad 2\alpha^2 = \frac{a_{66} + 2a_{12}}{2a_{11}} - \sqrt{\frac{a_{22}}{a_{11}}};$$
$$a_{11} = \frac{1}{E_L}; \quad a_{12} = \frac{-\nu_{LT}}{E_L}; \quad a_{22} = \frac{1}{E_T}; \quad a_{66} = \frac{1}{G_{LT}}; \quad (4)$$

where, $E, v,$ and G denote Young's modulus, Poisson's ratio and shear modulus respectively, L and T represent longitudinal and transverse directions respectively. In the absence of body forces, the stress components under mode I/II loading can be obtained from the functions $F_{I,II}$ (Eqs. (1) and (2)) as

$$(\sigma_x)_{I,II} = \partial^2 F_{I,II}/\partial y^2, \quad (\sigma_y)_{I,II} = \partial^2 F_{I,II}/\partial x^2, \quad (\tau_{xy})_{I,II} = -\partial^2 F_{I,II}/\partial x \partial y \tag{5}$$

The stress strain relations for a 2D orthotropic body under plane stress conditions are

$$\varepsilon_x = a_{11}\sigma_x + a_{12}\sigma_y, \quad \varepsilon_y = a_{12}\sigma_x + a_{22}\sigma_y \text{ and } \gamma_{xy} = a_{66}\tau_{xy} \tag{6}$$

Using Eqs. (5), (6) along with Eqs. (1) and (2), the strain components for mode I are

$$\begin{aligned}
\varepsilon_{xx} &= \frac{(\alpha-\beta)}{2\alpha}\left\{a_{12} - a_{11}(\alpha+\beta)^2\right\}\text{Re } Z_I(z_1) \\
&+ \frac{(\alpha+\beta)}{2\alpha}\left\{a_{12} - a_{11}(\beta-\alpha)^2\right\}\text{Re } Z_I(z_2) \\
&+ \frac{\beta}{2\alpha}\{a_{11}(\alpha+\beta)^2 - a_{12}\}\text{Re } Y_I(z_1) \\
&+ \frac{\beta}{2\alpha}\{a_{12} - a_{11}(\beta-\alpha)^2\}\text{Re } Y_I(z_2) \\
\varepsilon_{yy} &= \frac{(\alpha-\beta)}{2\alpha}\{a_{22} - a_{12}(\alpha+\beta)^2\}\text{Re } Z_I(z_1) \\
&+ \frac{(\alpha+\beta)}{2\alpha}\{a_{22} - a_{11}(\beta-\alpha)^2\}\text{Re } Z_I(z_2) \\
&+ \frac{\beta}{2\alpha}\{a_{12}(\alpha+\beta)^2 - a_{22}\}\text{Re } Y_I(z_1) \\
&+ \frac{\beta}{2\alpha}\{a_{22} - a_{12}(\beta-\alpha)^2\}\text{Re } Y_I(z_2) \\
\gamma_{xy} &= \frac{a_{66}}{2\alpha}(\alpha^2-\beta^2)\{\text{Im } Z_I(z_1) - \text{Im } Z_I(z_2)\} \\
&- \frac{a_{66}\beta}{2\alpha}\{(\beta+\alpha)\text{Im } Y_I(z_1) - (\beta-\alpha)\text{Im } Y_I(z_2)\}
\end{aligned} \tag{7}$$

and the strain components corresponding to mode II are

$$\begin{aligned}
\varepsilon_{xx} &= \frac{(1-\alpha)}{2\alpha}\left\{a_{11}(\alpha+\beta)^2 - a_{12}\right\}\text{Re } Y_{II}(z_1) \\
&- \frac{(1-\alpha)}{2\alpha}\{a_{11}(\beta-\alpha)^2 - a_{12}\}\text{Re } Y_{II}(z_2) \\
&+ \frac{1}{2\alpha}\left\{a_{11}(\alpha+\beta)^2 - a_{12}\right\}\text{Im } Y_{II}(z_1) \\
&- \frac{1}{2\alpha}\left\{a_{11}(\beta-\alpha)^2 - a_{12}\right\}\text{Im } Y_{II}(z_2) \\
\varepsilon_{yy} &= \frac{(1-\alpha)}{2\alpha}\left\{a_{12}(\alpha+\beta)^2 - a_{22}\right\}\text{Re } Y_{II}(z_1) \\
&- \frac{(1-\alpha)}{2\alpha}\left\{a_{12}(\beta-\alpha)^2 - a_{22}\right\}\text{Re } Y_{II}(z_2) \\
&+ \frac{1}{2\alpha}\left\{a_{12}(\alpha+\beta)^2 - a_{22}\right\}\text{Im } Z_{II}(z_1) \\
&- \frac{1}{2\alpha}\left\{a_{12}(\beta-\alpha)^2 - a_{22}\right\}\text{Im } Z_{II}(z_2) \\
\gamma_{xy} &= \frac{(1-\alpha)}{2\alpha}a_{66}\{(\beta-\alpha)\text{Im } Y_{II}(z_2) - (\beta+\alpha)\text{Im } Y_{II}(z_1)\} \\
&+ \frac{a_{66}}{2\alpha}\{(\beta+\alpha)\text{Re } Z_{II}(z_1) - (\beta-\alpha)\text{Re } Z_{II}(z_2)\}.
\end{aligned} \tag{8}$$

The complex analytical functions for opening mode, $Z_I(z_i)$ and $Y_I(z_i)$ and those for shearing mode, $Z_{II}(z_i)$ and $Y_{II}(z_i)$ are given by

$$Z_I(z_i)_{i=1,2} = \sum_{n=0}^{N} A_n z_i^{n-1/2} \qquad Y_I(z_i)_{i=1,2} = \sum_{m=0}^{M} B_m z_i^m$$
$$\text{and} \tag{9}$$
$$Z_{II}(z_i)_{i=1,2} = \sum_{n=0}^{N} C_n z_i^{n-1/2} \qquad Y_{II}(z_i)_{i=1,2} = \sum_{m=0}^{M} D_m z_i^m$$

Substitution of Eq. (9) in Eqs. (7) and (8) and superposition of mode I and mode II strain components leads to the exact representation of the strain field under mixed mode loading conditions. Considering a three parameter strain series for mode I (A_0, A_1, B_0) and mode II (C_0, C_1, D_0), the normal strain along aa' (Fig. 1) for a strain gage at point $P(r,\theta)$ may be written as

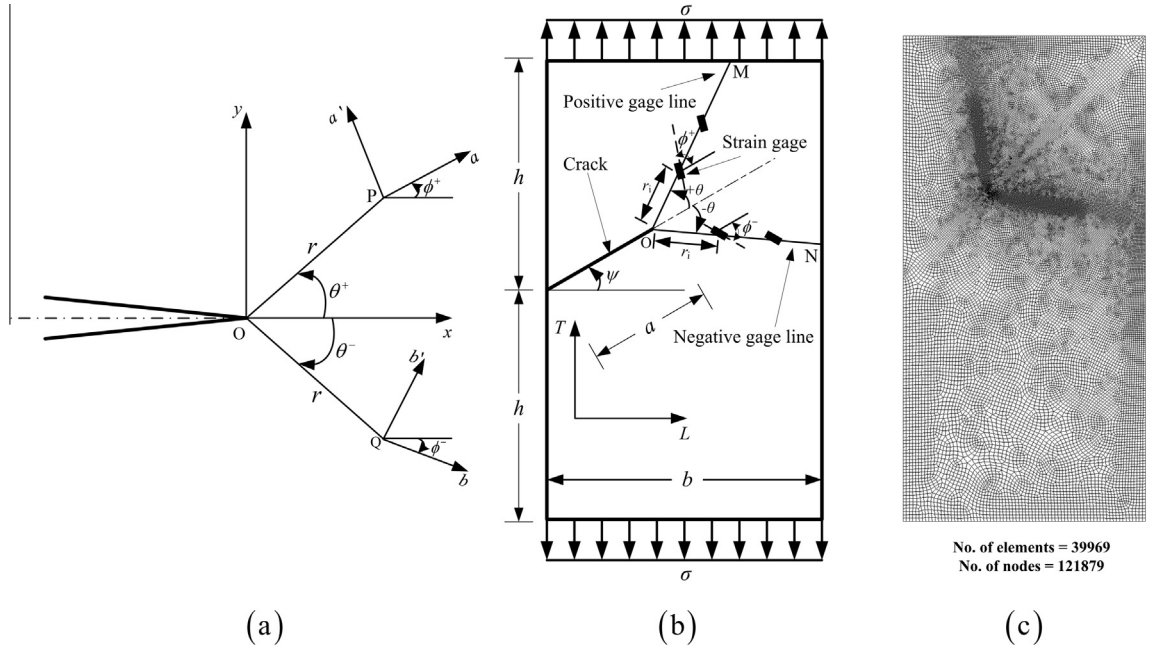

Fig. 1. (a) Co-ordinate system (b) slant edge cracked laminate specimen (c) typical FE mesh of the specimen.

$$
\begin{aligned}
&A_0\left\{\begin{array}{l}\left[\frac{1}{\sqrt{r_1}}\left(\left(\cos\frac{\theta_1}{2}\,\frac{\alpha-\beta}{2\alpha}\begin{pmatrix}(a_{12}\cos^2\phi+a_{22}\sin^2\phi)\\-(\beta+\alpha)^2(a_{11}\cos^2\phi+a_{12}\sin^2\phi)\end{pmatrix}\right)-\left(\sin\frac{\theta_1}{2}a_{66}\sin\phi\cos\phi\left(\frac{\alpha^2-\beta^2}{2\alpha}\right)\right)\right)\right]\\+\left[\frac{1}{\sqrt{r_2}}\left(\left(\cos\frac{\theta_2}{2}\,\frac{\alpha+\beta}{2\alpha}\begin{pmatrix}(a_{12}\cos^2\phi+a_{22}\sin^2\phi)\\-(\beta-\alpha)^2(a_{11}\cos^2\phi+a_{12}\sin^2\phi)\end{pmatrix}\right)+\left(\sin\frac{\theta_2}{2}a_{66}\sin\phi\cos\phi\left(\frac{\alpha^2-\beta^2}{2\alpha}\right)\right)\right)\right]\end{array}\right\}\\
&+A_1\left\{\begin{array}{l}\left[\sqrt{r_1}\left(\left(\cos\frac{\theta_1}{2}\,\frac{\alpha-\beta}{2\alpha}\begin{pmatrix}(a_{12}\cos^2\phi+a_{22}\sin^2\phi)\\-(\beta+\alpha)^2(a_{11}\cos^2\phi+a_{12}\sin^2\phi)\end{pmatrix}\right)+\left(\sin\frac{\theta_1}{2}a_{66}\sin\phi\cos\phi\left(\frac{\alpha^2-\beta^2}{2\alpha}\right)\right)\right)\right]\\+\left[\sqrt{r_2}\left(\left(\cos\frac{\theta_2}{2}\,\frac{\alpha+\beta}{2\alpha}\begin{pmatrix}(a_{12}\cos^2\phi+a_{22}\sin^2\phi)\\-(\beta-\alpha)^2(a_{11}\cos^2\phi+a_{12}\sin^2\phi)\end{pmatrix}\right)-\left(\sin\frac{\theta_2}{2}a_{66}\sin\phi\cos\phi\left(\frac{\alpha^2-\beta^2}{2\alpha}\right)\right)\right)\right]\end{array}\right\}
\end{aligned}
$$

$$
\begin{aligned}
\varepsilon_{aa} &= +B_0\left\{\frac{\beta}{2\alpha}\left[(\alpha+\beta)^2-(\beta-\alpha)^2\right]\left(a_{11}\cos^2\phi+a_{12}\sin^2\phi\right)\right\}\\
&+C_0\left\{\begin{array}{l}\left[\frac{1}{\sqrt{r_1}}\left(\left(\sin\frac{\theta_1}{2}\,\frac{1}{2\alpha}\begin{pmatrix}(\beta+\alpha)^2(a_{11}\cos^2\phi+a_{12}\sin^2\phi)\\-(a_{12}\cos^2\phi+a_{22}\sin^2\phi)\end{pmatrix}\right)+\left(\cos\frac{\theta_1}{2}a_{66}\sin\phi\cos\phi\left(\frac{\beta+\alpha}{2\alpha}\right)\right)\right)\right]\\-\left[\frac{1}{\sqrt{r_2}}\left(\left(\sin\frac{\theta_2}{2}\,\frac{1}{2\alpha}\begin{pmatrix}(\beta-\alpha)^2(a_{11}\cos^2\phi+a_{12}\sin^2\phi)\\-\left(a_{12}\cos^2\phi+a_{22}\sin^2\phi\right)\end{pmatrix}\right)-\left(\cos\frac{\theta_2}{2}a_{66}\sin\phi\cos\phi\left(\frac{\beta-\alpha}{2\alpha}\right)\right)\right)\right]\end{array}\right\}\\
&+C_1\left\{\begin{array}{l}\left[\sqrt{r_1}\left(\left(\sin\frac{\theta_1}{2}\,\frac{1}{2\alpha}\begin{pmatrix}(\beta+\alpha)^2(a_{11}\cos^2\phi+a_{12}\sin^2\phi)\\-(a_{12}\cos^2\phi+a_{22}\sin^2\phi)\end{pmatrix}\right)+\left(\cos\frac{\theta_1}{2}a_{66}\sin\phi\cos\phi\left(\frac{\beta+\alpha}{2\alpha}\right)\right)\right)\right]\\+\left[\sqrt{r_2}\left(\left(\sin\frac{\theta_2}{2}\,\frac{1}{2\alpha}\begin{pmatrix}(\beta-\alpha)^2(a_{11}\cos^2\phi+a_{12}\sin^2\phi)\\-(a_{12}\cos^2\phi+a_{22}\sin^2\phi)\end{pmatrix}\right)-\left(\cos\frac{\theta_2}{2}a_{66}\sin\phi\cos\phi\left(\frac{\beta-\alpha}{2\alpha}\right)\right)\right)\right]\end{array}\right\}\\
&+D_0\left\{\frac{1-\alpha}{2\alpha}\left[(\alpha+\beta)^2-(\beta-\alpha)^2\right](a_{11}\cos^2\phi+a_{12}\sin^2\phi)\right\}
\end{aligned}
\tag{10}
$$

Inspection of Eq. (10) indicates that terms containing B_0, D_0 become zero if

$$\tan\phi = -\frac{a_{11}}{a_{12}} \tag{11}$$

Again, terms containing A_1 will be zero if the coefficient of A_1 in Eq. (10) is made zero.

Using Eq. (4) in Eq. (10) and equating the coefficient of A_1 to zero leads to

$$
\begin{aligned}
&\sqrt[4]{\left(\cos^2\theta+(\beta+\alpha)^2\sin^2\theta\right)}\left\{\begin{array}{l}\left[\frac{1}{E_T}\left(\frac{1-\nu_{LT}\nu_{TL}}{1+\nu_{LT}}\right)\frac{\alpha-\beta}{2\alpha}\cos\left(\frac{1}{2}\left(\tan^{-1}((\beta+\alpha)\tan\theta)\right)\right)\right]\\-\left[\frac{1}{G_{LT}}\left(\frac{\nu_{LT}}{(1+\nu_{LT})\sqrt{\nu_{TL}}}\right)\frac{1}{2\alpha}\sin\left(\frac{1}{2}\left(\tan^{-1}((\beta+\alpha)\tan\theta)\right)\right)\right]\end{array}\right\}\\
&+\sqrt[4]{\left(\cos^2\theta+(\beta-\alpha)^2\sin^2\theta\right)}\left\{\begin{array}{l}\left[\frac{1}{E_T}\left(\frac{1-\nu_{LT}\nu_{TL}}{1+\nu_{LT}}\right)\frac{\alpha+\beta}{2\alpha}\cos\left(\frac{1}{2}\left(\tan^{-1}((\beta-\alpha)\tan\theta)\right)\right)\right]\\+\left[\frac{1}{G_{LT}}\left(\frac{\nu_{LT}}{(1+\nu_{LT})\sqrt{\nu_{TL}}}\right)\frac{1}{2\alpha}\sin\left(\frac{1}{2}\left(\tan^{-1}((\beta-\alpha)\tan\theta)\right)\right)\right]\end{array}\right\}=0
\end{aligned}
\tag{12}
$$

Solution of Eq. (12) gives the values of θ for which coefficient of A_1 becomes zero. Using θ from Eq. (12) and ϕ from Eq. (11), the strain expression ε_{aa} contains only the terms with coefficients A_0, C_0 and C_1. The normal strain ε_{aa} at a point with radial location r, on the positive gage line (+ve values of θ and ϕ)) and the normal strain ε_{bb} at a point with radial location r on the negative gage line ($-$ve values of θ and ϕ) (Fig. 1(a)) can be written as

$$
\begin{aligned}
&A_0\left\{\begin{array}{l}\left(a_{12}\cos^2\phi+a_{22}\sin^2\phi\right)\left(\frac{\alpha-\beta}{2\alpha}\,\frac{1}{\sqrt{r_1}}\cos\frac{\theta_1}{2}+\frac{\alpha+\beta}{2\alpha}\,\frac{1}{\sqrt{r_2}}\cos\frac{\theta_2}{2}\right)\\+\left[a_{66}\sin\phi\cos\phi\left(\frac{\alpha^2-\beta^2}{2\alpha}\right)\right]\left(\frac{1}{\sqrt{r_2}}\sin\frac{\theta_2}{2}-\frac{1}{\sqrt{r_1}}\sin\frac{\theta_1}{2}\right)\end{array}\right\}\\
&\varepsilon_{aa,bb} = \pm C_0\left\{\begin{array}{l}\frac{1}{2\alpha}(a_{12}\cos^2\phi+a_{22}\sin^2\phi)\left(\frac{1}{\sqrt{r_1}}\sin\frac{\theta_1}{2}-\frac{1}{\sqrt{r_2}}\sin\frac{\theta_2}{2}\right)\\+\left(\frac{a_{66}\sin\phi\cos\phi}{2\alpha}\right)\left[\frac{(\beta+\alpha)}{\sqrt{r_1}}\cos\frac{\theta_1}{2}-\frac{(\beta-\alpha)}{\sqrt{r_2}}\cos\frac{\theta_2}{2}\right]\end{array}\right\}\\
&\pm C_1\left\{\begin{array}{l}\frac{1}{2\alpha}(a_{12}\cos^2\phi+a_{22}\sin^2\phi)\left(\sqrt{r_2}\sin\frac{\theta_2}{2}-\sqrt{r_1}\sin\frac{\theta_1}{2}\right)\\+\left(\frac{a_{66}\sin\phi\cos\phi}{2\alpha}\right)\left[(\beta+\alpha)\sqrt{r_1}\cos\frac{\theta_1}{2}-(\beta-\alpha)\sqrt{r_2}\cos\frac{\theta_2}{2}\right]\end{array}\right\}
\end{aligned}
\tag{13}
$$

where, + sign and $-$ sign correspond to ε_{aa} and ε_{bb} respectively. Thus, a strain gage placed at a radial distance r from the crack tip on a line making an angle of θ and gage orientation ϕ either on the positive or the negative gage line with the crack axis measures strains containing only the terms A_0, C_0 and C_1. Using relations from Eq. (4) in Eq. (13) and adding ε_{aa} and ε_{bb} and multiplying with $\sqrt{r}$ results in

$$\frac{(\varepsilon_{aa}+\varepsilon_{bb})\sqrt{r}}{I_1}=A_0 \tag{14}$$

which contains only coefficient pertaining to mode I loading. Similarly, subtracting ε_{bb} from ε_{aa} (from Eq. (13)) and multiplying with $\sqrt{r}$ using Eq. (4) gives

$$\frac{(\varepsilon_{aa}-\varepsilon_{bb})\sqrt{r}}{I_2}=C_0+\frac{C_1 r}{I_2}I_3 \tag{15}$$

which now contains only coefficients relating to mode II loading. Here, I_1, I_2 and I_3 are functions of the material properties $(E_L, E_T, \nu_{LT}, G_{LT})$ and θ and ϕ. The coefficients A_0 and C_0 are determined from the best fit plots of the quantities on the L.H.S of Eqs. (14) and (15) which in turn can be used to estimate the mixed mode SIFs (K_I, K_{II}) as

$$K_I=\sqrt{2\pi}A_0 \text{ and } K_{II}=\sqrt{2\pi}C_0 \tag{16}$$

2.2. Determination of maximum permissible radial location r_{max}

In cracked orthotropic materials, the minimum radial distance ahead of the crack tip for pasting strain gages to avoid 3D effects [21] is

$$r_{min}=\text{thickness of the specimen } (t) \tag{17}$$

The maximum radial distance of the strain gages from the crack tip, r_{max} is the extent of validity of the three parameter strain series represented by Eq. (13) along the positive and negative gage lines. However, this may be different along the positive (r^+_{max}) and negative (r^-_{max}) gage lines and the maximum permissible radial distance is

$$r_{max}=\text{minimum}\left[r^+_{max}, r^-_{max}\right] \tag{18}$$

Consequently, the optimal or valid radial locations r_i for all strain gages are given by

$$r_{min}\leqslant r_i\leqslant r_{max} \tag{19}$$

The quantities on LHS of Eqs. (14) and (15) are computed from the ε_{aa} and ε_{bb} values evaluated at radial locations along the positive and negative gage lines (OM and ON in Fig. 1(b)) using finite element analysis (FEA) of a given cracked configuration. The values of the coefficients A_0, C_0 and C_1 are obtained using the best-fit regression of the plots of Eqs. (14) and (15). Using these values, the RHS quantities of Eq. (13) are compared with the LHS quantities obtained from FEA (i.e. ε_{aa} and ε_{bb}) by plotting against the radial distance from the crack tip for all the points on the positive and negative gage lines. The point of deviation of the RHS of Eq. (13) from finite element (FE) values of ε_{aa} and ε_{bb} (determined using a relative error criterion of 1%) gives r^+_{max} (along positive gage line) and r^-_{max} (along negative gage line) and r_{max} is obtained from Eq. (18). From, Eqs. (14) and (15) it is clear that two strain gages are to be pasted on each gage line within the estimated r_{max} for the determination of K_I and K_{II} using the proposed technique.

3. Numerical results and discussions

For the slant edge cracked plates (SECP) subjected to uniform tensile stress (Fig. 1(b)), r_{max} values have been determined and numerical simulations have been performed for determination of mixed mode SIFs of orthotropic materials using the proposed method. The FEA for all the configurations have been performed using commercial FE software ANSYS® [38] employing eight noded isoparametric elements and collapsed quarter point elements have been used to capture the $\sqrt{r}$ singularity around the crack tip [39]. Two types of SECP laminates viz. $[0_2/90]_{2S}$ and $[0/\pm45/90]_S$ made of glass epoxy have been considered. In order to understand the effect of crack inclination angle (ψ) and relative crack size (a/b) on r_{max} and to study the efficacy of the present method in determination of mixed mode SIFs over a wider range of crack configurations, different values of ψ and a/b are considered for both the laminates. The applied load, material and geometric parameters for all the specimens considered in all the examples are listed in Table 1. Corresponding to these properties, the values of gage orientation, ϕ (from Eq. (11)) and gage line orientation, θ (from Eq. (12)) are calculated as 68.01° and 54.27°, respectively for the $[0_2/90]_{2S}$ glass-epoxy SECP laminate. Similarly, for the$[0/\pm45/90]_S$glass epoxy SECP laminate the values of gage orientation, ϕ and gage line orientation, θ are calculated as 61.13° and 64.5°, respectively. Fig. 1(c) shows a typical finite element mesh used where the bottom edge of the plate is completely constrained and a uniform tensile stress is applied on the top edge. Consecutive nodes along the positive and negative gage lines are at equal distances from the crack tip simulating the strain gages to be pasted at equal distances (Eqs. (14) and (15)).

3.1. Example 1: General procedure for determination of r_{max}

In order to validate the proposed approach and to demonstrate the general procedure of determination of r_{max}, for the accurate measurement of mixed mode SIFs using strain gages, SECPs made of $[0_2/90]_{2S}$ and$[0/\pm45/90]_S$glass epoxy with $\psi=45°$ and $a/b=0.5$ are considered in this section. Other properties corresponding to these configurations are given in Table 1.

Following the procedure described in Section 2.2, the values of strains, ε_{aa} and ε_{bb} of the nodes along the positive and negative gage lines are obtained from the FEA. Fig. 2(a) and (b) show the plots of $(\varepsilon_{aa}+\varepsilon_{bb}/I_1)\sqrt{r}$ and $(\varepsilon_{aa}-\varepsilon_{bb}/I_2)\sqrt{r}$ respectively versus radial distance (r) with their respective straight line fits for the $[0_2/90]_{2S}$ glass-epoxy SECP. The values of the coefficients A_0, C_0 and C_1 for the best fit plots along with the correlation coefficient (R^2) are also shown in Fig. 2(a) and (b). It can be noticed from Fig. 2(a) that the slope of the best fit line to the data is almost nearer to zero as predicted by the theory. Fig. 2(c) and (d) show the comparison of the strain values ε_{aa} and ε_{bb} along the positive and negative gage lines respectively obtained from the FEA and those obtained using Eq. (13). It may be pointed out that the coefficients used in Eq. (13) are obtained from the best fit plots in Fig. 2 (a) and (b). As the estimated coefficients are accurate, both ε_{aa} and ε_{bb} variations along gage line are congruent to those obtained from Eq. (13) in Fig. 2(c) and (d) respectively till the point of deviation.

For the $[0_2/90]_{2S}$ glass-epoxy SECP, the radii corresponding to the points of deviation between the FE strains and the best fit strains along the positive gage line (r^+_{max}) and along the along the negative gage line (r^-_{max}) are shown in Fig. 2(c) and (d). These (r^+_{max}) and (r^-_{max}) represent the extents of validity of the three

Table 1
Geometric, loading and material parameters for the specimens (Ref. Fig. 1).

Laminate Specification	b(mm)	a/b	h/b	ν_{LT}	E_L (GPa)	E_T (GPa)	G_{LT} (GPa)	σ (MPa)	t (mm)
$[0_2/90]_{2S}$ Glass-epoxy	150	0.2–0.7	1	0.163	33.3	24.6	5.2	1	1
$[0/\pm45/90]_S$ Glass-epoxy				0.304	23.24	23.24	8.91		

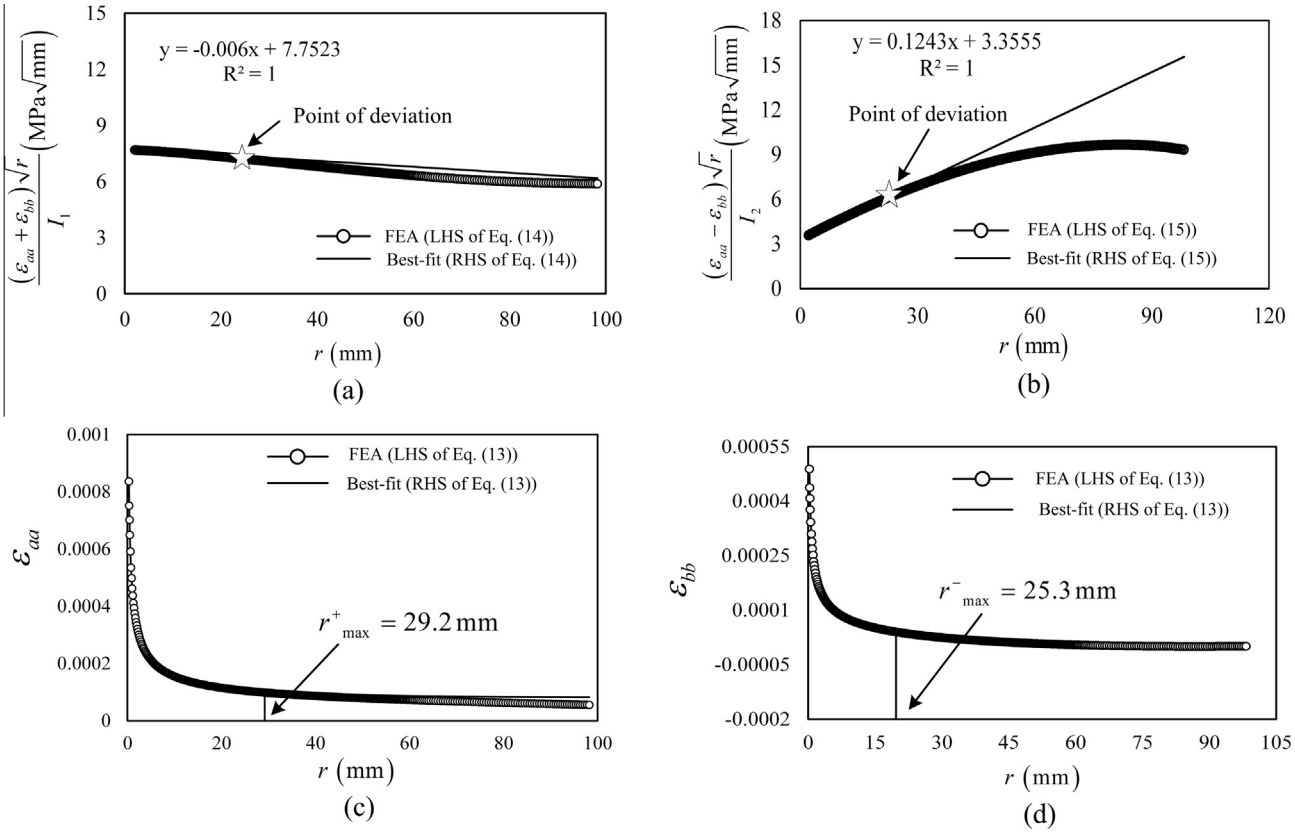

Fig. 2. Plots for $[0_2/90]_{2S}$ glass-epoxy SECP with $a/b = 0.5$: Determination of (a) A_0 (b) C_0 and C_1, (c) r^{+}_{max} and (d) r^{-}_{max}.

parameter strain series along the positive and negative gage lines respectively. In this case r^{+}_{max} is 29.2 mm and r^{-}_{max} is 25.3 mm and following Eq. (18), the r_{max} is 25.3 mm within which the strain gages should be pasted along both the gage lines for accurate estimation of SIFs. The value of r_{max} has been arrived at after conducting proper convergence study using various gradations of mesh density. Following the same steps, the plots of $(\varepsilon_{aa} + \varepsilon_{bb}/I_1)\sqrt{r}$ and $(\varepsilon_{aa} - \varepsilon_{bb}/I_2)\sqrt{r}$ versus radial distance (r) and the plots of ε_{aa} and ε_{bb} along the positive and negative gage lines are obtained from the FEA as shown in the Fig. 3(a-d). Form these plots, the values r^{+}_{max} (=18.35 mm) and r^{-}_{max} (=26.5 mm) are obtained as shown in Fig. 3(c-d) and following Eq. (18), the value of r_{max} for the $[0/\pm 45/90]_S$ glass-epoxy SECP is obtained as 18.35 mm.

3.2. Example 2: Validation of the strain gage technique for the determination of mixed mode SIFs

In order to numerically simulate the strain gage based determination of K_I and K_{II} following the proposed method using four strain gages (two along positive gage line and two along negative gage line), strain values at nodes along the gage lines are considered to be strain gage readings. Using these strain values, SIFs have been calculated using Eqs. (14)–(16). For this purpose, the configurations analyzed in Example 1 are considered here. Further, to understand the importance of r_{max} on the accuracy of determination of SIFs, these strains (representing strain gage readings) are obtained for five different combinations of strain gage placements starting with case 1, where both the strain gages along the gage lines are placed within r_{max} (following Eq. (19)) till case 5, where both the strain gages are placed outside r_{max} and other three intermediate combinations. These combinations are shown in Tables 2 and 3 for the laminates $[0_2/90]_{2S}$ and $[0/\pm 45/90]_S$ respectively.

The values of K_I and K_{II} determined employing the displacement extrapolation technique using nodal displacement values of the crack tip elements obtained from FEA [40] for the $[0_2/90]_{2S}$ glass-epoxy SECP is found to be 19.17 MPa$\sqrt{\text{mm}}$ and 8.27 MPa$\sqrt{\text{mm}}$ respectively. For the $[0/\pm 45/90]_S$ glass-epoxy SECP the values of K_I and K_{II} are found to be 19.24 MPa$\sqrt{\text{mm}}$ and 8.68 MPa$\sqrt{\text{mm}}$ respectively. These values are used as reference solutions to test the accuracy of the simulated values of K_I and K_{II} determined employing the proposed technique. Tables 2 and 3 show the% relative error of the numerically simulated K_I and K_{II} values with the reference solutions for all the five cases of strain gage placement for the SECP laminates $[0_2/90]_{2S}$ and $[0/\pm 45/90]_S$respectively. It could be observed that in both the laminates, the errors in K_I/K_{II} measurement are very low when the strain gages (simulated by nodal strains ε_{aa} and ε_{bb}) are placed within r_{max} (optimal gage locations) and the errors are much higher when the strain gages are placed outside r_{max}. In the case of $[0_2/90]_{2S}$ SECP K_I, K_{II} laminate, the minimum error is as low as 0.52% and the maximum error is as high as 22.2%. On the other hand for $[0/\pm 45/90]_S$SECP laminate, the minimum and maximum errors are 0.69% and 29.03% respectively. It was also observed that even when one of the strain gages is placed outside r_{max}, keeping the other within r_{max} (along both the gage lines) the error jumps from a mere value of 2.4–9.7%. This shows that the placement of strain gages within r_{max} following the proposed Eq. (19) is of utmost importance for accurate estimation of SIFs.

3.3. Example 3: Determination of K_I, K_{II} and r_{max} for different mixed mode configurations

Using the present method, mixed mode SIFs (K_I and K_{II}) for the SECPs made of $[0_2/90]_{2S}$ and $[0/\pm 45/90]_S$glass-epoxy laminates

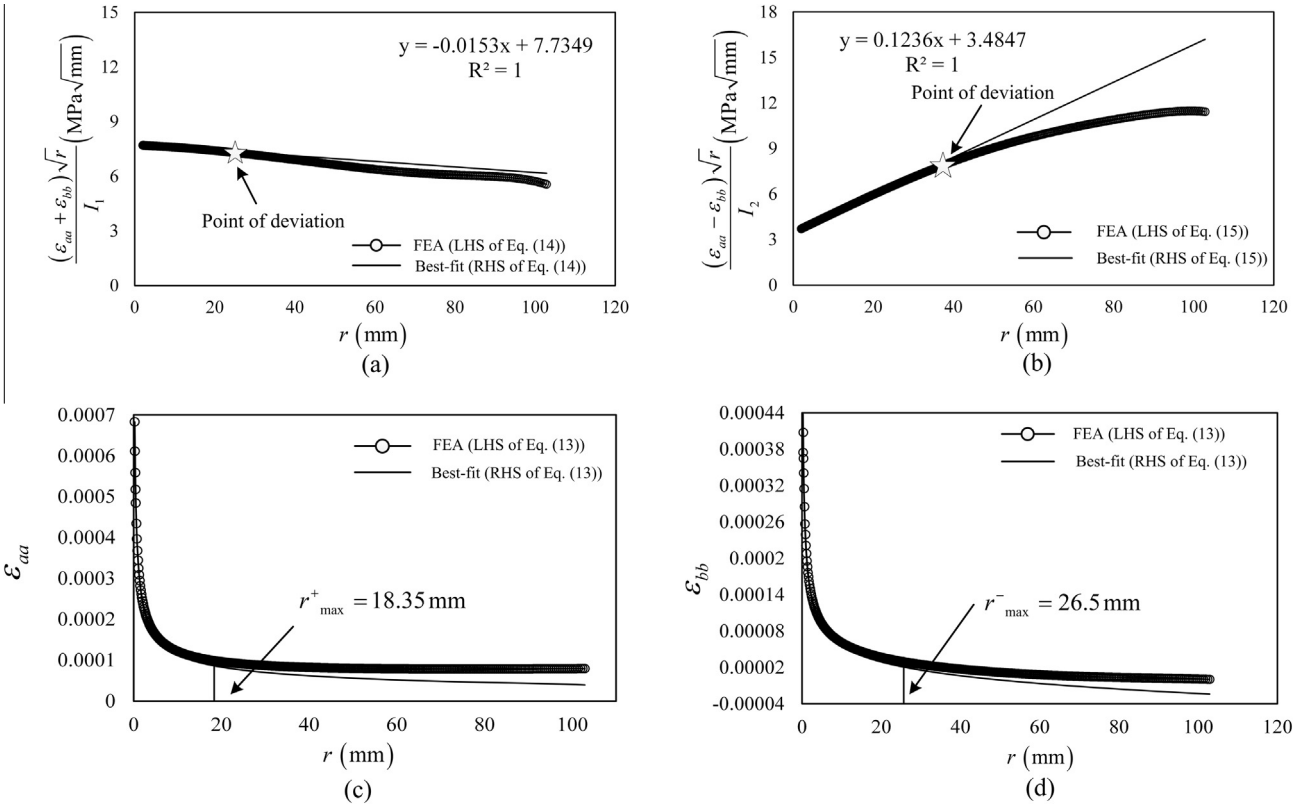

Fig. 3. Plots for $[0/\pm 45/90]_S$ glass-epoxy SECP with $a/b = 0.5$: Determination of (a) A_0 (b) C_0 and C_1, (c) r^{+}_{max} and (d) r^{-}_{max}.

Table 2
K_I and K_{II} obtained for different cases of strain gage placements for $[0_2/90]_{2S}$ glass-epoxy SECP laminate ($r_{max} = 25.3$ mm; $a/b = 0.5$; $\psi = 45^0$; $K_{Iref} = 19.17$ MPa$\sqrt{\text{mm}}$; $K_{IIref} = 8.27$ MPa$\sqrt{\text{mm}}$).

Case	r_1 and r_2 (mm)	ε_{aa}	ε_{bb}	K_I (MPa $\sqrt{\text{mm}}$)	% Rel. err.	K_{II} (MPa $\sqrt{\text{mm}}$)	% Rel. err.
1	$r_1 = 7.03$	1.81E−04	8.82E−04	19.07	0.52	8.35	0.91
	$r_2 = 10.23$	1.53E−04	6.86E−04				
2	$r_1 = 10.23$	1.53E−04	6.86E−04	19.00	0.91	8.39	1.51
	$r_2 = 12.28$	1.41E−04	5.99E−04				
3	$r_1 = 12.28$	1.41E−04	5.99E−04	18.92	1.31	8.47	2.42
	$r_2 = 17.15$	1.22E−04	4.53E−04				
4	$r_1 = 17.15$	1.22E−04	4.53E−04	17.72	7.58	9.07	9.69
	$r_2 = 30.0$	9.72E−05	2.40E−05				
5	$r_1 = 30.0$	9.72E−05	2.40E−05	17.32	9.67	10.10	22.12
	$r_2 = 36.0$	9.01E−05	1.79E−05				

Table 3
K_I and K_{II} obtained from different cases of strain gage placements for $[0/\pm 45/90]_S$ glass-epoxy laminate ($r_{max} = 18.3$ mm; $a/b = 0.5$; $\psi = 45^0$; $K_{Iref} = 19.24$ MPa$\sqrt{\text{mm}}$; $K_{IIref} = 8.68$ MPa$\sqrt{\text{mm}}$).

Case	r_1 and r_2 (mm)	ε_{aa}	ε_{bb}	K_I (MPa $\sqrt{\text{mm}}$)	% Rel. err.	K_{II} (MPa $\sqrt{\text{mm}}$)	% Rel. err.
1	$r_1 = 6.23$	1.81E−04	8.82E−04	19.12	0.62	8.74	0.69
	$r_2 = 8.06$	1.53E−04	6.86E−04				
2	$r_1 = 8.06$	1.53E−04	6.86E−04	19.04	1.04	8.54	1.61
	$r_2 = 11.16$	1.41E−04	5.99E−04				
3	$r_1 = 11.16$	1.41E−04	5.99E−04	18.94	1.56	8.42	2.99
	$r_2 = 14.7$	1.22E−04	4.53E−04				
4	$r_1 = 14.7$	1.22E−04	4.53E−04	18.2	5.40	9.41	8.41
	$r_2 = 25.2$	9.72E−05	2.40E−05				
5	$r_1 = 25.2$	9.72E−05	2.40E−05	17.14	10.91	11.2	29.03
	$r_2 = 30.5$	9.01E−05	1.79E−05				

(Fig. 1(b)) with $a/b = 0.5$ are determined for $\psi = 15^\circ - 75^\circ$ (in steps of 15°) and are compared with the reference values as shown in Table 4. Here, in each case, both the strain gages (simulated by nodal strain) along both the gage lines are considered to be placed within the respective r_{max}. Fig. 4(a) and (b) show the variations of K_I and K_{II} with ψ obtained using the present technique for $a/b = 0.5$ for $[0_2/90]_{2S}$ glass-epoxy and$[0/\pm 45/90]_S$ glass-epoxy SECP laminates respectively. Similar trends in the variation of K_I and K_{II} with ψ have also been observed for other values of a/b. In all the cases, K_I decreases steadily with the increase in ψ, whereas K_{II} increases and reaches a maximum at $\psi = 45^\circ$, and then decreases as expected [41] thus again reinforcing efficacy of the present approach. Values of and K_{II} obtained using the numerical simulation of the present method for both the laminated SECP for different values of crack inclination angle, ψ along with the errors are listed in Table 4. The results in Table 4 clearly show that highly accurate values of both K_I and K_{II} can be obtained using the proposed strain gage technique over a wide range of crack inclination angle. Fig. 5(a) and (b) show the variation in r_{max}/b with ψ for different a/b ratios for $[0_2/90]_{2S}$ and $[0/\pm 45/90]_S$ glass epoxy SECP

Table 4
Mixed mode SIFs for different crack inclination angle for $[0_2/90]_{2S}$ and $[0/\pm 45/90]_S$ glass-epoxy laminates.

Laminate Specification	Angle, ψ	K_I (MPa $\sqrt{mm}$)			K_{II} (MPa $\sqrt{mm}$)		
		Present method	Ref. value	% Rel. error	Present method	Ref. value	% Rel. error
$[0_2/90]_{2S}$ Glass-epoxy	15°	39.22	39.15	0.19	5.43	5.31	2.25
	30°	30.1	29.93	0.58	7.75	7.59	2.11
	45°	19.25	19.17	0.39	8.27	8.14	1.59
	60°	10.78	10.57	1.89	6.84	6.72	1.78
	75°	4.19	4.06	2.99	3.83	3.74	2.41
$[0/\pm 45/90]_S$ Glass-epoxy	15°	39.39	39.38	0.02	5.45	5.52	1.26
	30°	29.72	29.8	0.27	7.73	7.58	1.97
	45°	19.12	19.24	0.62	8.73	8.68	0.57
	60°	10.39	10.5	1.06	7.00	6.87	1.89
	75°	4.27	4.21	1.42	3.89	3.95	1.51

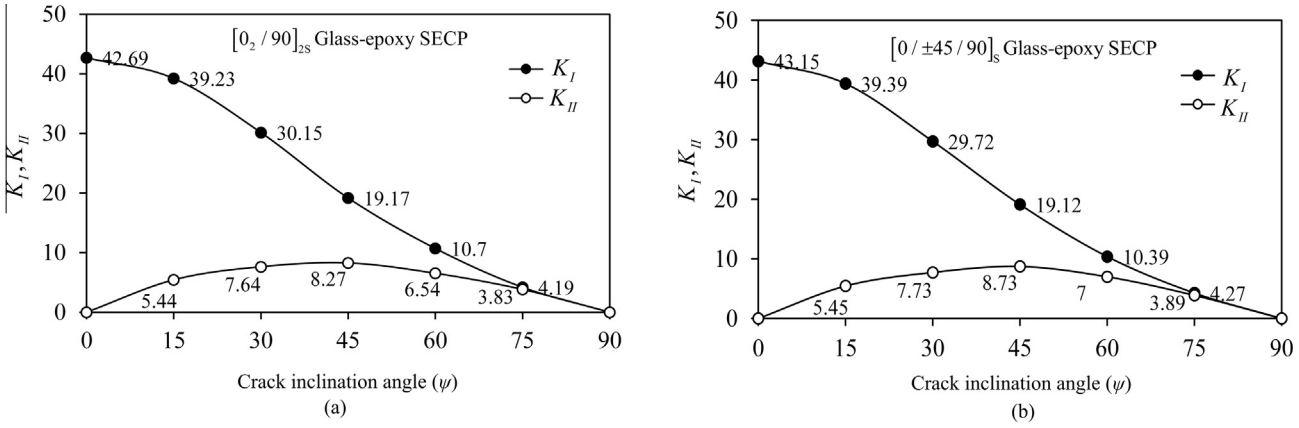

Fig. 4. Variation of K_I and K_{II} (MPa$\sqrt{mm}$) with crack inclination angles (ψ) for (a) $[0_2/90]_{2S}$ glass-epoxy SECP; (b) $[0/\pm 45/90]_S$ glass-epoxy SECP.

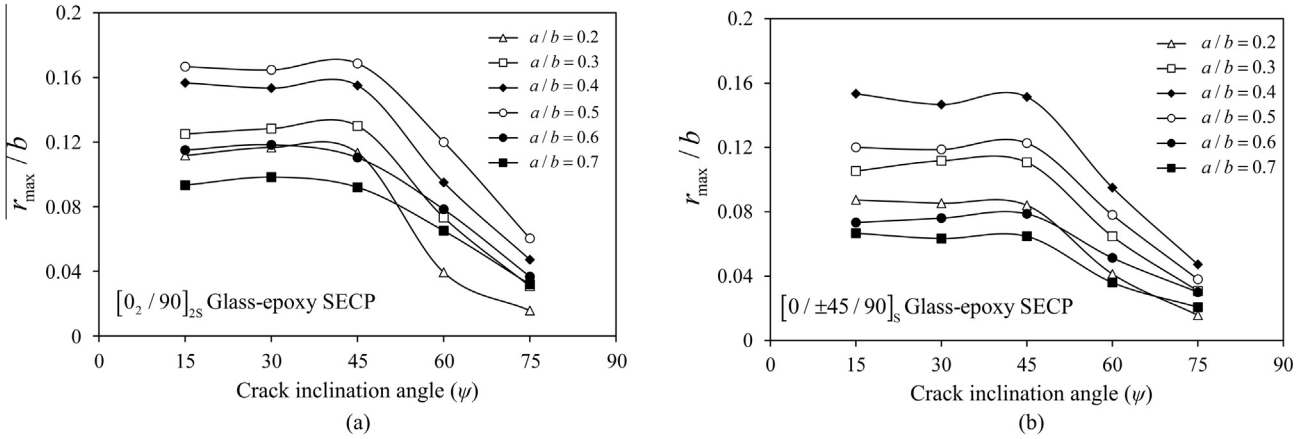

Fig. 5. Variation of r_{max}/b with crack inclination angles (ψ) for different a/b for (a) $[0_2/90]_{2S}$ glass-epoxy SECP; (b) $[0/\pm 45/90]_S$ glass-epoxy SECP.

Table 5
Variation of the r_{max}/b with a/b of the $[0_2/90]_{2S}$ and $[0/\pm45/90]_S$ glass-epoxy SECP configuration with $\psi = 45^\circ$

Laminate Specification	a/b	$r_{max}(mm)$	r_{max}/b
$[0_2/90]_{2S}$ Glass-epoxy	0.2	17	0.113
	0.3	19.5	0.13
	0.4	23.2	0.155
	0.5	25.3	0.168
	0.6	16.6	0.110
	0.7	13.8	0.092
$[0/\pm45/90]_S$ Glass-epoxy	0.2	12.6	0.084
	0.3	16.6	0.11
	0.4	22.7	0.151
	0.5	18.4	0.123
	0.6	11.8	0.079
	0.7	9.7	0.065

laminates respectively. In both the cases of SECP laminates, it may be observed that for a particular a/b ratio, though initially r_{max} is almost independent of, it shows a gradual decline with further increase in ψ. For the SECP, as the crack inclination angle increases, the positive gage line moves towards the boundary edges. However, up to $\psi = 45^\circ$, the boundary effects being negligible, there is minimal or no variation in r_{max}. But beyond 45°, the positive gage line inches much closer towards the boundary and therefore, there is a decline in the r_{max} value with increase in ψ due to significant boundary effects.

Apart from ψ, the a/b ratio also affects the values of r_{max} and hence the valid gage locations. For example, Table 5 shows the r_{max} values with different a/b for $\psi = 45^\circ$ for both $[0_2/90]_{2S}$ and $[0/\pm45/90]_S$ glass epoxy SECP laminates. The variation of r_{max}/b with a/b for different values of ψ for $[0_2/90]_{2S}$ and $[0/\pm45/90]_S$ glass epoxy SECP laminates are shown in Fig. 6(a) and (b) respectively and in the both the cases the trends followed are same as reported by Chakraborty et al. [24,25] for mode I configurations. The value of r_{max} increases with increasing a/b, reaches a maximum and decreases as the crack tip approaches boundary leading to inverted bell shaped curves. It may be attributed to the fact that at low values of a/b when there is insignificant boundary effects, the changes in r_{max} is controlled by changes in a/b. However, as the crack tip proceeds towards the outer boundaries, the net ligament length decreases and a point is reached when the controlling parameter is shifted from the crack length to the net ligament, $b - a$ and r_{max} decreases.

4. Conclusions

A simple, robust and practically feasible strain gage technique has been developed for the first time for the accurate determination of mixed mode SIFs (K_I and K_{II}) in orthotropic laminates. The proposed theoretical framework not only allows determination of mixed mode SIFs (K_I and K_{II}) using strain gages in orthotropic materials but also allows to calculate the valid radial locations of the strain gages ensuring accurate determination of K_I and K_{II}. As the proposed strain gage technique depends on three parameter representation, it allows the gages to be placed reasonably far away from the crack tip. Further, the proposed technique needs only four strain gages for determination of mixed mode SIFs. A finite element based methodology is also developed to evaluate the extent of radial locations of the strain gages (r_{max}) which ensure accurate determination of K_I and K_{II} for orthotropic laminates. Numerical experimentations have been performed on $[0_2/90]_{2S}$ and $[0/\pm45/90]_S$ glass- epoxy SECP laminates to validate the developed theory. Results show that the strains computed at points within r_{max} follow the theoretical predictions which validate the proposed method. It was observed that r_{max} depends both on the crack inclination angle (ψ) and on the relative crack length (a/b). Up to $\psi = 45^\circ$, r_{max} remains almost same but beyond that r_{max} shows a sharp decrease. For a given ψ, r_{max} initially increases with the increase in a/b and then decreases. Numerical simulations show that while the computed values of K_I and K_{II} obtained from the simulated readings of strain gages placed within r_{max} are highly accurate, a very high error ({>}29%) results when the gages are placed outside r_{max}. Simulations have been carried out to show the robustness of the proposed method over a range of crack inclination angles. An extremely important recommendation from the present study is that while conducting strain gage based experiments, the radial locations where the strain gages need to be placed are dependent on the crack configurations (relative crack size and crack angle) and arbitrarily placing the strain gages will lead to highly erroneous results. The present work provides a robust method for prior determination of such optimal locations for a given configuration. The proposed method will be immensely useful for experimental stress analysts in accurate determination of mixed mode SIFs in orthotropic composites using strain gages as the r_{max} value for a given configuration could be easily calculated using a simple FEA.

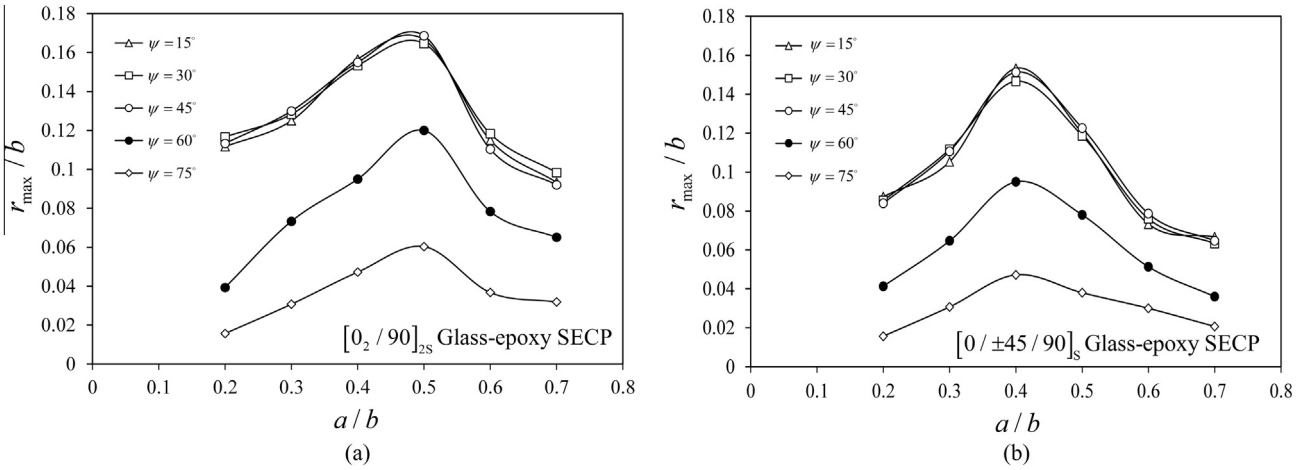

Fig. 6. Variation of r_{max}/b with a/b for different ψ for (a) $[0_2/90]_{2S}$ glass-epoxy SECP; (b) $[0/\pm45/90]_S$ glass-epoxy SECP.

References

[1] Irwin GR. Analytical aspects of crack stress field problems. T&AM Report No. 213, Urbana: University of Illinois; 1962.
[2] Wu EM. On the application of fracture mechanics to orthotropic plates. T&AM Report No. 248, Urbana: University of Illinois; 1963.
[3] Sih GC, Paris PC, Irwin GR. On cracks in rectilinearly anisotropic bodies. Int J Fract Mech 1965;1:189–203.
[4] Dharan CKH. Fracture mechanics of composite materials. J Eng Mater Technol 1978;100:233–47.
[5] Sharokh Parhizgar, Zachary LW, Sun CT. Application of linear elastic fracture mechanics to composite materials. Int J Fract 1982;20:3–15.
[6] Rossmanith HP, Linsbauer HN. Analysis of mode.1 crack-tip stress patterns in orthotropic materials. Ing Arch 1985;55:258–66.
[7] Nobile L, Carloni C. Fracture analysis of orthotropic cracked plates. Compos Struct 2005;68:285–93.
[8] Kim JH, Paulino GH. Mixed-mode fracture of orthotropic functionally graded materials using finite elements and the modified crack closure method. Eng Fract Mech 2002;69:1557–86.
[9] Asadpoure A, Mohammadi S. A new approach to simulate the crack with the extended finite element method in orthotropic media. Int J Numer Methods Eng 2007;69:2150–72.
[10] Fantuzzi N, Dimitri R, Tornabene F. A SFEM-based evaluation of mode-I Stress Intensity Factor in composite structures. Compos Struct 2016;145:162–85.
[11] Baik MC, Choi SH, Hawong JS, Kwon JD. Determination of stress intensity factors by the method of caustics in anisotropic materials. Exp Mech 1995;35:137–43.
[12] Yao X, Chen J, Jin G, Arakawa K, Takahashi K. Caustic analysis of stress singularities in orthotropic composite materials with mode-I crack. Compos Sci Technol 2004;64:917–24.
[13] Mojtahed M, Zachary LW. Use of photoelasticity to determine orthotropic K_I stress-intensity factor. Exp Mech 1987;27:184–9.
[14] Ju SH, Liu SH. Determining stress intensity factors of composites using crack opening displacement. Compos Struct 2007;81:614–21.
[15] Khanna SK, Ellingsen MD, Winter RM. Investigation of fracture in transparent glass fiber reinforced polymer composites using photoelasticity. J Eng Mater Technol 2004;126:1–7.
[16] Mogadpalli GP, Parameswaran V. Determination of stress intensity factor for cracks in orthotropic composite materials using digital image correlation. Strain 2008;44:446–52.
[17] Dally JW, Sanford RJ. Strain gage methods for measuring the opening mode stress intensity factor. Exp Mech 1987;27:381–8.
[18] Berger JR, Dally JW. An over deterministic approach for measuring K_I using strain gages. Exp Mech 1988;28:142–5.
[19] Wei J, Zhao JH. A two-strain-gage technique for determining mode I stress intensity factor. Theoret Appl Fract Mech 1997;28:135–40.
[20] Dally JW, Barker DB. Dynamic measurement of initiation toughness at high loading rates. Exp Mech 1988;28:298–303.
[21] Shukla A, Agarwal BD, Bhushan B. Determination of stress intensity factor in orthotropic materials using strain gages. Eng Fract Mech 1989;32:469–77.
[22] Khanna SK, Shukla A. Development of stress field equations and determination of stress intensity factor during dynamic fracture of orthotropic composite materials. Eng Fract Mech 1994;47:345–59.
[23] Cerniglia D, Nigrelli V, Pasta A. Experimental and numerical determination of stress intensity factor in composite material. In: Conference proceedings ICCM-12, Europe, 1999, paper 932.
[24] Debaleena Chakraborty, Murthy KSRK, Chakraborty D. A new single strain gage technique for determination of mode I stress intensity factor in orthotropic composite materials. Eng Fract Mech 2014;124–125:142–54.
[25] Debaleena Chakraborty, Murthy KSRK, Chakraborty D. Determination of K_I in orthotropic laminates with double ended cracks using a single strain gage technique. Theoret Appl Fract Mech 2016;82:96–106.
[26] Harvey CM, Wood JD, Wang S, Watson A. A novel method for the partition of mixed-mode fractures in 2D elastic laminated unidirectional composite beams. Compos Struct 2014;116:589–94.
[27] Wood JD, Harvey CM, Wang S. Partition of mixed-mode fractures in 2D elastic orthotropic laminated beams under general loading. Compos Struct 2016;149:239–46.
[28] Dally JW, Riley WF. Experimental stress analysis. Singapore: McGraw; 1991.
[29] Dally JW, Berger JR. A strain gage method for determining K_I and K_{II} in a mixed mode stress field, In: The proceedings of the 1986 SEM Spring conference on experimental mechanics, New Orleans, LA, 1986. p. 603–612.
[30] Dorogoy A, Rittel WF. Optimum location of a three strain gauge rosette for measuring mixed mode stress intensity factors. Eng Fract Mech 2008;75:4127–39.
[31] Sarangi H, Murthy KSRK, Chakraborty D. Optimum strain gage locations for accurate determination of the mixed mode stress intensity factors. Eng Fract Mech 2012;88:63–78.
[32] Rosakis J, Ravi-Chandar K. On crack-tip stress state: an experimental evaluation of three-dimensional effects. Int J Solids Struct 1986;22:121–34.
[33] Mahishi JM, Admas DE. Energy Release Rate During Delamination Crack Growth in Notched Composite Laminates. In: John Son WS, editor. Delamination and debonding of materials, ASTM, STP 876, American Society for Testing of Materials, Philadelphia, 1985, p. 95–111.
[34] Bakis CE, Yih HR, Stinchcomb WW, Reifsnider KL. Damage initiation and growth in notched laminates under reversed cyclic loading. composite materials: fatigue and fracture. In: Lagace PA editor, 2nd Volume, ASTM STP 102; 1989. p. 66–83.
[35] Jen MHR, Kau YS, Hsu JM. Initiation and propagation of delamination in a centrally notched composite laminate. J Compos Mater March 1993;27:272–302.
[36] Irwin GR. Analysis of stresses and strains near the end of a crack traversing a plate. J Appl Mater 1957;24:361–4.
[37] Sanford RJ. A critical re-examination of the Westergaard method for solving opening-mode crack problems. Mech Res Commun 1979;6:289–98.
[38] ANSYS, Theory reference manual, Release 11, Swanson Analysis Systems Inc; 2007.
[39] Barsoum RS. On the use of isoparametric finite elements in linear fracture mechanics. Int J Numer Methods Eng 1976;10:25–37.
[40] Ayhan AO, Kaya AC, Loghin A, Laflen JH, McClain RD, Slavik D. Fracture Analysis of cracks in orthotropic materials using ANSYS®. In: Conference proceedings GT 2006 (ASME Turbo Expo 2006: Power for Land, Sea and Air), Spain; 2006.
[41] Mohammadi S. XFEM fracture analysis of composites. John Wiley and Sons Ltd; 2012.